Journal of Biomolecular NMR (2005) 31: 185–199
DOI 10.1007/s10858-005-0165-1

Structure of calmodulin complexed with an olfactory CNG channel fragment and role of the central linker: Residual dipolar couplings to evaluate calmodulin binding modes outside the kinase family

Gian Marco Contessa[a,c], Maria Orsale[a], Sonia Melino[a], Vincent Torre[d], Maurizio Paci[a,c], Alessandro Desideri[b,c,*] & Daniel O. Cicero[a,d,*]
[a]*Department of Chemical Sciences and Technologies;* [b]*Department of Biology;* [c]*INFM, University of Rome "Tor Vergata", via della Ricerca Scientifica, 00133, Rome, Italy;* [d]*INFM and SISSA, Settore di Biofisica, Trieste, Italy*

Received 8 September 2004; Accepted 22 December 2004

Key words: backbone dynamics, calmodulin, calmodulin binding modes, NMR, olfactory CNG channel, residual dipolar couplings

Abstract

The NMR high-resolution structure of calmodulin complexed with a fragment of the olfactory cyclic-nucleotide gated channel is described. This structure shows features that are unique for this complex, including an active role of the linker connecting the N- and C-lobes of calmodulin upon binding of the peptide. Such linker is not only involved in the formation of an hydrophobic pocket to accommodate a bulky peptide residue, but it also provides a positively charged region complementary to a negative charge of the target. This complex of calmodulin with a target not belonging to the kinase family was used to test the residual dipolar coupling (RDC) approach for the determination of calmodulin binding modes to peptides. Although the complex here characterized belongs to the (1–14) family, high Q values were obtained with all the 1:1 complexes for which crystalline structures are available. Reduction of the RDC data set used for the correlation analysis to structured regions of the complex allowed a clear identification of the binding mode. Excluded regions comprise calcium binding loops and loops connecting the EF-hand motifs.

Introduction

Residual dipolar couplings (RDCs) are receiving an increasing attention for the structure characterization of biomolecules by NMR (Bax, 2003). Their use as structural constraints can improve both precision and accuracy of structure determination in solution. Unlike other more classical NMR structural parameters, like NOEs and scalar couplings, RDCs data can be regarded as long-range structural constraints. As an alternative to their application as additional constraints during structure calculation, RDCs can be used to validate a structural model, derived from a high-resolution X-ray structure of a homologous protein (Tjandra et al., 1997; Bewley et al., 1998; Clore and Gronenborn, 1998). By using RDC data one can quickly and reliably assess protein structural features without embarking in the more time consuming approach that involves NOE and J coupling data for structure calculation. The characterization of the binding mode of calmodulin (CaM) to its biological target is one example in which RDCs can give a significant contribution to accelerate structure classification.

*To whom correspondence should be addressed. E-mail: cicero@scienze.uniroma2.it; desideri@uniroma2.it

CaM is a small calcium-binding protein that exerts a large variety of biological functions in the cell. Crystal and NMR structures of CaM in complex with fragments of CaM-regulated proteins have been reported, revealing that there are multiple mechanisms of interaction between CaM and its targets (Vetter and Leclerc, 2003). The first examples refer to peptides derived from different protein kinases (Ikura et al., 1992; Meador et al., 1992), where CaM forms a wrap-around structure, providing a channel that accommodates the helical peptide target. Based on these structures, three different families of binding modes were established (1–14, 1–10 and 1–16), depending on the distances between key hydrophobic residues or anchors (Yap et al., 2000). The structural features of the first group, having 12 residues between the two anchors, are similar to those found in the smMLCK (Meador et al., 1992) or skMLCK (Ikura et al., 1992) complexes, whereas the second group (having 8 residues between the anchors) shares common features with CaMKII (Meador et al., 1993). The (1–16) motif, characterized by the presence of 14 residues between the two hydrophobic anchors, is, to this date, represented only by the CaMKK complex (Kurokawa et al., 2001).

From a structural point of view, a comparison of the three types of complexes reveals that they mainly differ in the relative orientation of the two lobes. By defining axes of closure, bend and twist, it was calculated that conversion of the (1–14) N-lobe orientation into the (1–10), while superimposing the C-lobe, would require 17° closure, −3° bend and 8° twist (Mal et al., 2002). Transformation between the (1–16) and the (1–10) N-lobe orientations requires even more extensive rotations of 40°, 5° and −13° for closure, bend, and twist, respectively (Mal et al., 2002). This feature prompted the use of RDCs as a convenient tool to classify kinases binding modes by NMR (Mal et al., 2002). This method has been used to build plausible structural models for CaM complexed with CaMKIp and CaMKIVp for which no structures were available, allowing the classification of both targets as (1–14). The assumption underlying this application is that the structural differences among the three types of CaM complexes (namely 1–10, 1–14 and 1–16) are greater than those between the unknown structure and the model template. Binding differences are, however, likely to exist due to the low sequence conservation of CaM targets (Rhoads and Friedberg, 1997). The success in the classification of CaMKIp and CaMKIVp seems to ensure that the assumption is fulfilled for targets belonging to the protein kinase family, but no attempt was made to extend this approach to other targets. Analysis of the recently determined structure of CaM complexed with a peptide derived from the endothelial nitric oxide synthase (eNOSp) already predicted possible difficulties, when considering peptides not belonging to the kinase fragments (Aoyagi et al., 2003). Although the primary structure of eNOSp presents all the key residues for a 1–14 interaction, attempts to solve the structure through molecular replacement, with the smMLCKp structure, failed. In fact, the determined structure shows significant deviations (more than 2.6 Å) from that of the 1–14 kinase complex. This structure variability, which is a remarkable example of CaM plasticity in its capability to adapt to very different target sequences raises a fundamental question. Are the three known structures of CaM with the three kinase fragments sufficient to ensure a rapid classification using the RDC approach? In the present work we try to provide a first answer to this question studying the interaction of CaM with a peptide derived from the olfactory cyclic nucleotide-gated (CNG) channel.

CaM is known to interact with both rod and olfactory CNG channels producing a modulation of their activity (Molday, 1996). As far as the olfactory CNG channel is concerned, the binding region has been identified in the N-terminal domain of the α-subunit (Liu et al., 1994). Actually, a 26-aminoacid synthetic peptide (bOCNCp, Figure 1) corresponding to residues 62–87 of the channel was shown to present a high affinity for CaM (K_d 4–12 nM), in the same range of the observed EC50 of CaM (21 nM) (Liu et al., 1994). This region is also involved in the N-term–C-term interaction that occurs within the channel, suggesting that CaM can modulate the channel by disrupting the interaction between the N- and C-terminal domain (Varnum and Zagotta, 1997). The interaction of bOCNC with CaM has been studied by NMR and found to follow a 1:1 stoichiometry and to involve both lobes of CaM (Orsale et al., 2003). Analysis of the primary structure of bOCNCp reveals the presence of two aromatic residues in relative position 1 and 14 (Figure 1). It also exhibits in position 10 another

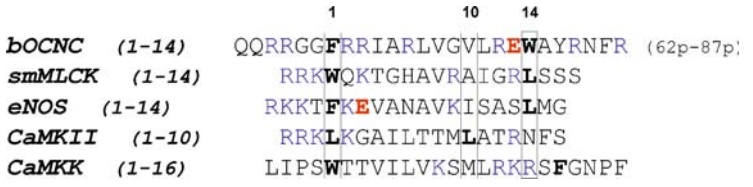

Figure 1. Alignment of the sequences of CaM-binding region of the olfactory CNG channel, smMLCK, eNOS, CaMKII and CaMKK, based on the position of the N-terminal key residue. Key hydrophobic residues are in bold. Acidic and basic residues are shown in red and blue, respectively.

hydrophobic residue that can act as anchor, leading to a (1–10) type of interaction (residue 5 in this case is alanine, part of the consensus sequence for this motif). In fact, a peptide lacking the last 8 residues, and hence without the tryptophan, was observed to still bind CaM (Liu et al., 1994). To clarify the structural details of the CaM–bOCNCp interaction we have solved the high resolution structure of the complex using multidimensional and multinuclear NMR, and measured the backbone mobility of the complex through ^{15}N relaxation measurements. Finally, we have tested the ability of RDCs alone to assess the binding mode of calmodulin to a peptide that does not belong to the kinase family.

Materials and methods

Sample preparation

Uniformly ^{15}N- or $^{15}N/^{13}C$-labeled recombinant *Xenopus laevis* CaM (identical to mammalian CaM) was prepared following the classical procedures (Putkey et al., 1985). bOCNCp was purchased from Epytop (France).

NMR spectroscopy

NMR experiments were performed at 35 °C on Bruker Avance 700-MHz spectrometer equipped with a triple resonance probe incorporating self-shielded gradient coils. Pulsed field gradients were appropriately employed to achieve suppression of the solvent signal and spectral artifacts. Quadrature detection for the indirectly detected dimensions was obtained using the States–TPPI method. The NMR data were processed and analyzed on Silicon Graphics workstations using NMRPipe (Delaglio et al., 1995) and NMRView (Johnson and Blevins, 1994) programs. Linear prediction and apodization 90°-shifted squared sine-bell functions were typically applied before Fourier transformation.

Concentration of the ^{15}N uniformly and $^{15}N/^{13}C$ uniformly labeled protein were 0.4–1.2 mM. NMR samples were prepared in $CaCl_2$ 6 mM and KCl 140 mM, pH 6.7.

Assignments of the ^{1}H, ^{15}N, ^{13}CO and ^{13}C resonances of the CaM–bOCNCp complex were already reported in a previous publication (Orsale et al., 2003).

In order to collect the NOEs, 3D ^{15}N-edited NOESY and ^{13}C-edited NOESY were acquired using a mixing time of 100 ms. A 2D ^{15}N, ^{13}C-filtered NOESY spectrum (Ikura and Bax, 1992) and a 3D ^{13}C F1-edited, F3-filtered HMQC-NOESY (Lee et al., 1994) experiment were performed to reveal only contacts involving the unlabeled peptide.

A set of $^{3}J_{HNH\alpha}$ was determined by measuring cross peak intensities in the HNHA spectrum. $^{1}H-^{15}N$ dipolar couplings were recorded using a two-dimensional IPAP-type (in phase/antiphase) (Ottiger et al., 1997; Bax et al., 2001) $^{1}H-^{15}N$ HSQC correlation experiment. The samples used for RDC measurements also contain 16 mg/mL filamentous phage Pf1 (Asla Labs) to induce the molecular alignment. Amide chemical shifts of all CaM–peptide complexes in the Pf1 liquid crystal are very similar to those measured in isotropic samples, indicating that perturbation of the protein structure by the alignment medium is minimal.

Structure calculation

Structure calculation and refinement were performed with XPLOR (version 3.85) using a simulated annealing protocol, modified in order to incorporate RDC, a direct potential for J scalar

couplings and a refinement against a database of Ramachandran plot dihedral angles (Brunger, 1992; Tjandra et al., 1997; Clore et al., 1998).

The ensemble of the 20 lowest-energy target function structures was chosen to represent the solution structure. The programs AQUA and PROCHECK (Laskowski et al., 1996) were used to analyze the structures.

Approximate interproton distances were derived and the corresponding restraints were subdivided into three groups:1.8–3.2 Å for strong NOEs, 1.8–3.8 Å for medium NOEs and 1.8–6.5 Å for weak NOEs.

In addition, backbone ϕ torsional angle was restrained to $-60° \pm 40°$ for residues exhibiting $^{3}J_{HNH\alpha} < 6.0$ Hz and to $-120° \pm 50°$ for residues exhibiting $^{3}J_{HNH\alpha} > 8.0$ Hz, while for all remaining residues ϕ angle was restrained to negative values ($-90° \pm 80°$), except for glycine residues ($\phi = 90° \pm 80°$). Only in the later stages of the structural calculation, when it was possible to identify defined secondary structure elements, ψ angles were restrained to $-40° \pm 30°$ for α-helical regions.

The full list of atomic contacts of CaM with ligand Calcium atoms was taken from literature (Babu et al., 1988).

In the α-helix regions hydrogen bonds were added evaluating the spatial relationships of the protons with potential acceptors in the initial structures calculated without the use of any hydrogen bond restraint.

A set of 93 $^{1}H-^{15}N$ RDCs for CaM was included in the refinement, ranging from 40.5 Hz to −39.3 Hz, with an accuracy of 2.0 Hz. Fitting of the observed RDCs to the smMLCKp complex using the singular value decomposition (SVD) method (Fischer et al., 1999; Losonczi et al., 1999) within the PALES program (Zweckstetter and Bax, 2000), provided an initial guess for the magnitude and orientation of the molecular alignment tensor. Subsequent optimization during the simulated annealing process (Bryce and Bax, 2004) led to the following final values: $Da^{NH} = -19.74$ Hz and R = 0.56.

In order to carry out a complete cross-validation of RDCs, a series of simulated annealing calculations were performed, each of them lacking 10% of the RDCs (randomly chosen from the whole dataset) (Clore and Garrett, 1999). By means of the SVD method the missing RDCs in each run were back-calculated, in order to check how well every RDC can be predicted, and an average R_{free} of 0.25 was obtained.

Relaxation data and backbone dynamics

Relaxation experiments were carried out at 35 °C on the Bruker Avance700 spectrometer mentioned before. Measurements of ^{15}N T_1, T_2 and $^{1}H-^{15}N$ NOE were performed at 70.94 MHz ^{15}N frequency using standard pulse schemes (Kay et al., 1989; Barbato et al., 1992) in an interleaved manner to collect six points with delays of 16, 142, 422, 702, 1192, 1543 ms for T_1 and 8.16, 24.48, 40.80, 57.12, 73.44, 97.92 ms for T_2. Data were fitted using the Rate Analysis routine of NMRView (Johnson and Blevins, 1994). The uncertainties in the peak intensities were evaluated as the standard deviation of the spectral noise measured in a region free of crosspeaks. The heteronuclear NOE values were determined by the ratio of peak volumes of spectra recorded with and without ^{1}H saturation, employing a net relaxation delay of 5 s for each scan in both experiments.

^{15}N relaxation data were analyzed in terms of model-free formalism, making use of the programs DASHA and DIFFC (Orekhov et al., 1995). With the aid of the latter we have calculated the hydrodynamics properties expected for the average structure of the CaM–bOCNCp complex. The resulting diffusion tensor has relative values of 1:0.8:0.7 for the D_{zz}, D_{yy} and D_{xx} components, respectively, suggesting only a moderate anisotropy for the global tumbling of the molecule. Moreover, there are no significant differences in the T_2 values measured for the different helices of the complexed calmodulin. This is an indication that the global tumbling can be considered as isotropic. In fact, different T_2s, which depend on the different angle that each helix makes with respect to the main axis of the diffusion tensor, are expected in the presence of anisotropic tumbling (Tjandra et al., 1995). In a first approximation, the T_1/T_2 ratio was used to estimate the isotropic τ_m (Farrow et al., 1994). Only those residues showing neither significant shortening of T_2 nor a $^{1}H-^{15}N$ NOE value less than 0.6 were used to derive τ_m.

In the second step, the relaxation quantities measured for each HN were analyzed using the

simple model-free formalism developed by Lipari and Szabo (1982). In this approach, a global τ_m and two parameters, S^2 and τ_e describing dynamic motions are extracted from the equations relating the T_1, T_2 and $^1H-^{15}N$ NOE to the spectral density function (Kay et al., 1989). Additionally, the 'extended' model free approach (Clore et al., 1990a) was also used for those residues that could not be fitted with the normal three-parameters model-free method. In this case, the five-parameter model was converted into a three-parameter model by constraining τ_f to 0 and by fixing τ_m to the value obtained for the other residues. Experimental data were fitted assuming four models: (a) S^2, (b) S^2, R_{ex}, (c) S^2, t_e, (d) S_f, S_s, t_s. Residues presenting the best fit with model (a) don't show any significant local mobility. Other regions show internal mobility that can be slower (model b) or faster (model c) than the global tumbling, or a combination of two internal motions (model d), one similar to the global tumbling and a faster one (Clore et al., 1990a). Statistical considerations regarding the fitting improvement and the number of freedom degrees were used to assign each residue to one of these classes.

In the last step, the statistically best fitting model for each individual residue was used to optimize τ_m by minimizing a single penalty function measuring the deviation between calculated and measured relaxation rates. A global correlation time of 7.63 ± 0.03 ns could be estimated.

F-test statistics

An F-test was performed upon the RDC data to discriminate between the different classical binding modes. The statistic was obtained from the relation $F = (\chi_i^2/\sigma_i^2)/(\chi_j^2/\sigma_j^2)$, where χ_k is the root-mean square deviation (rmsd) between experimental and calculated values, fitting RDC data from the entire CaM, while σ_k is the average rmsd from fitting RDC data using only N- or C-terminal domains of CaM, and the index k denotes the specific crystal structure used for comparison. Probabilities are evaluated making use of the facility at http://davidmlane.com/hyperstat/F_table.html.

Results and discussion

Structure of the CaM–bOCNCp complex

Assignment of the resonances belonging to the CaM–bOCNCp complex have been already presented (Orsale et al., 2003). For CaM and bound bOCNCp, 3028 and 38 distance restraints were obtained, respectively. The latter were measured using a 2D F1,F2-filtered NOESY experiment. Eighty-four NOEs were unambiguously assigned to intermolecular short distances. In the aromatic region of the 3D ^{13}C F1-edited, F3-filtered HMQC-NOESY experiment a large number of contacts (52) that F7p and W20p establish with CaM have been observed. Further structural constraints arose from the measurement of 68 $^3J_{HNH\alpha}$ coupling constants. One hundred and fifteen backbone $^1H-^{15}N$ RDCs of the complex in a liquid crystalline medium containing 16 mg/ml of filamentous phage Pf1 (Hansen et al., 1998) have been measured. Ninety-three RDCs belonging to residues showing no significant internal motion (see below) were used as well as 133 short distances for amide protons hydrogen-bonded to backbone carbonyls.

The 20 lowest energy-structures, shown in Figure 2, display a good overall convergence, since the backbone and heavy atoms show a rmsd with respect to the mean structure of 0.60 and 1.05 Å, respectively (see Table 1). The region comprising residues 1–5 and 146–148 of CaM, as well as the first and the last five residues of bOCNCp (62p–66p, 83p–87p) are ill-defined, indicating the presence of significant flexibility. The mobility of the peptide regions was confirmed by the large intensities of cross-peaks belonging to these residues observed in a F1,F2-filtered TOCSY (data not shown). The average structure for the CaM–bOCNCp complex shows the occurrence of the expected eight helices for bound CaM: E7–L18 (Helix I), T29–L39 (Helix II), E45–V55 (Helix III), F65–K77 (Helix IV), all in the N-lobe; S81–D93 (Helix V), A102–L112 (Helix VI), D118–A128 (Helix VII), Y138–T146 (Helix VIII) in the C-lobe. Short β-sheets are formed by interaction of strands located in the N-lobe (G25-T29 and G61–F65) and the C-lobe (Q135–Y138 and Y99–A102), connecting the two EF-hand motifs in each of the two lobes. Bound bOCNCp shows a helical conformation that extends from F68p to Y83p. Close contacts between consecutive NHs were readily observed in the 2D F1,F2-filtered

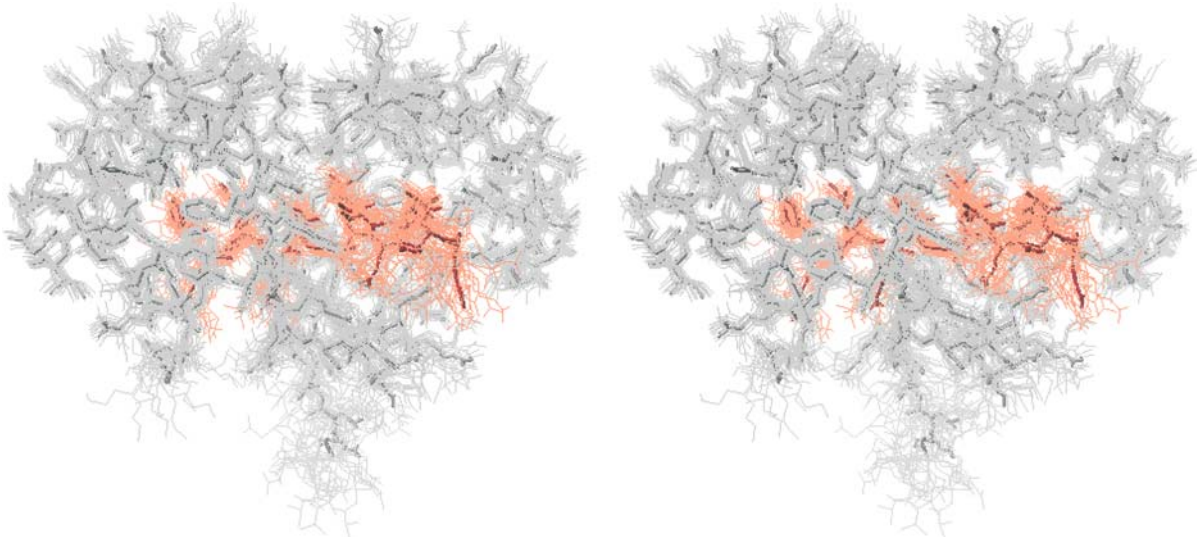

Figure 2. Stereoview of the 20 lowest-energy structures (in grey), superimposed to their average structure (in black). Only heavy atoms are shown. Bound bOCNCp is shown in red.

NOESY. The peptide is positioned in an antiparallel orientation in which F68p and W81p make prevalently contacts with the C-lobe and the N-lobe, respectively (Figure 3a).

Bound CaM shows the typical tunnel necessary to accommodated the target peptide (Ikura et al., 1992; Meador et al., 1992). Figure 3b shows the surface representation of the N-lobe of CaM with the main hydrophobic and electrostatic interactions. The peptide conformation determines the existence of several contacts between the N- and C-lobes (Figure 3a). One peculiarity of this structure is Helix IV that, spanning from residue F65 to residue K77, is longer than that observed in other CaM complexes, leaving a very short linker (about four residues) connecting the two lobes in the complex. The presence of an helix extending up to K77 is supported by a NOE between K77 HN and R74 Hα as well as the values of HNHα coupling constants of M76 (3.6 Hz) and K77 (5.4 Hz). This feature, together with the presence of M76 ε-Me intermolecular NOEs, indicates the presence of an extra hydrophobic pocket: a clear intermolecular contact involves M76 of CaM and V77p of bOCNCp. Several intermolecular NOEs were observed for V77p (Figure 3a), suggesting that it can be considered as a third key hydrophobic residue in the interaction with CaM and one can then assume a 1–10–14 interaction. A similar way of binding was also detected in the CaM–eNOSp complex, where the presence of a bulky amino acid at position 10 causes a longer Helix IV, and a series of hydrophobic interactions (Aoyagi et al., 2003). In both the eNOSp and bOCNCp complexes M76 is used by CaM, together with the other eight methionines, as a hydrophobic finger to contact the target at the bulky residue in position 10.

In our case, however, there is a second peculiarity of the target peptide leading to a more active role for the linker region. Actually, just before the second anchor of bOCNCp, the negatively charged residue, E80p, is significantly close to K75, inducing an electrostatic interaction. Remarkably, the linker region of CaM presents the only cluster of positively charged residues (R74, K75 and K77) in the whole protein. The structure of the CaM–bOCNCp complex shows how the negative charge of E80p can be conveniently accommodated close to the linker, and provides an example of electrostatic complementarity between CaM and its target: the peptide is constrained to be in an antiparallel orientation. The parallel orientation of bOCNCp would allow the occurrence of many hydrophobic interactions similar to those observed in other complexes (see Figure 1), while its antiparallel orientation is mainly due to the need of locating E80p in a favourable environment, suggesting that electrostatic interaction is the most important factor in defining the orientation of the CaM-target (Osawa et al., 1999).

Table 1. Experimental restraints and structural statistics for the 20 lowest-energy structures

Number of experimental restraints	3935	
Distance restraints from NOEs	3050	
Hydrogen bond distance restraints	133	
Backbone dihedral angle restraints	591	
HN-Hα scalar J coupling constants	68	
H-N residual dipolar coupling constants	93	
Average number of restraints per residue	24	
XPLOR energies (kcal/mol)		
E_{total}	3413.3 ± 48.4	
E_{bond}	27.73 ± 1.03	
E_{angle}	252.4 ± 7.1	
$E_{improper}$	57.58 ± 2.71	
E_{vdw}	91.67 ± 2.81	
E_{NOE}	175.1 ± 8.7	
E_{cdih}	1.04 ± 0.76	
E_{coup}	45.85 ± 3.83	
E_{sani}	22.15 ± 1.12	
E_{rama}	2739.8 ± 50.2	
RMS deviations from experimental restraints		
Average distance restraints violation (Å)	0.041 ± 0.001	
Average dihedral angle restraints violation (deg)	0.23 ± 0.10	
Average scalar J coupling constant violation (Hz)	0.82 ± 0.03	
Average RDC constant violation (Hz)	0.48 ± 0.01	
R_{free} (%)	0.25 ± 0.04	
RMS deviations from idealized covalent geometry		
Bond	0.00325 ± 0.00006	
Angle	0.592 ± 0.008	
Improper	0.529 ± 0.012	
Ramachandran analysis (res. 5–146, 66p–84p)		
Residues in favored regions (%)	96.26 ± 0.76	
Residues in additional allowed regions (%)	3.71 ± 0.76	
Residues in generously allowed regions (%)	0.04 ± 0.16	
Residues in disallowed regions (%)	0.0 ± 0.0	
Coordinates precision		
	backbone (Å)	all heavy atoms (Å)
residues 5–146, 66p–84p	0.60 ± 0.06	1.05 ± 0.07

Comparison with other 1–14 CaM complexes

The average structure for CaM–bOCNCp is a clear example of the plasticity used by CaM to adapt itself to different target sequences. The C-lobe is remarkably similar to that observed for the other two CaM–smMLCKp (Meador et al., 1992) and CaM–eNOSp (Aoyagi et al., 2003) 1–14 complexes but specific differences exist at the level of the N-lobe, especially with respect to the eNOSp complex (Table 2). These differences are mainly due to a negative charge in the eNOSp sequence, which shifts Helix I to avoid an unfavourable interaction between E14 of CaM and E498 of eNOSp (Aoyagi et al., 2003).

Superposition of the backbone atoms of the C-lobe for the three complexes, shown in Figure 4, indicates that, when looking at the relative position of the target peptide, eNOSp is shifted with respect to both bOCNCp and smMLCKp, to avoid the

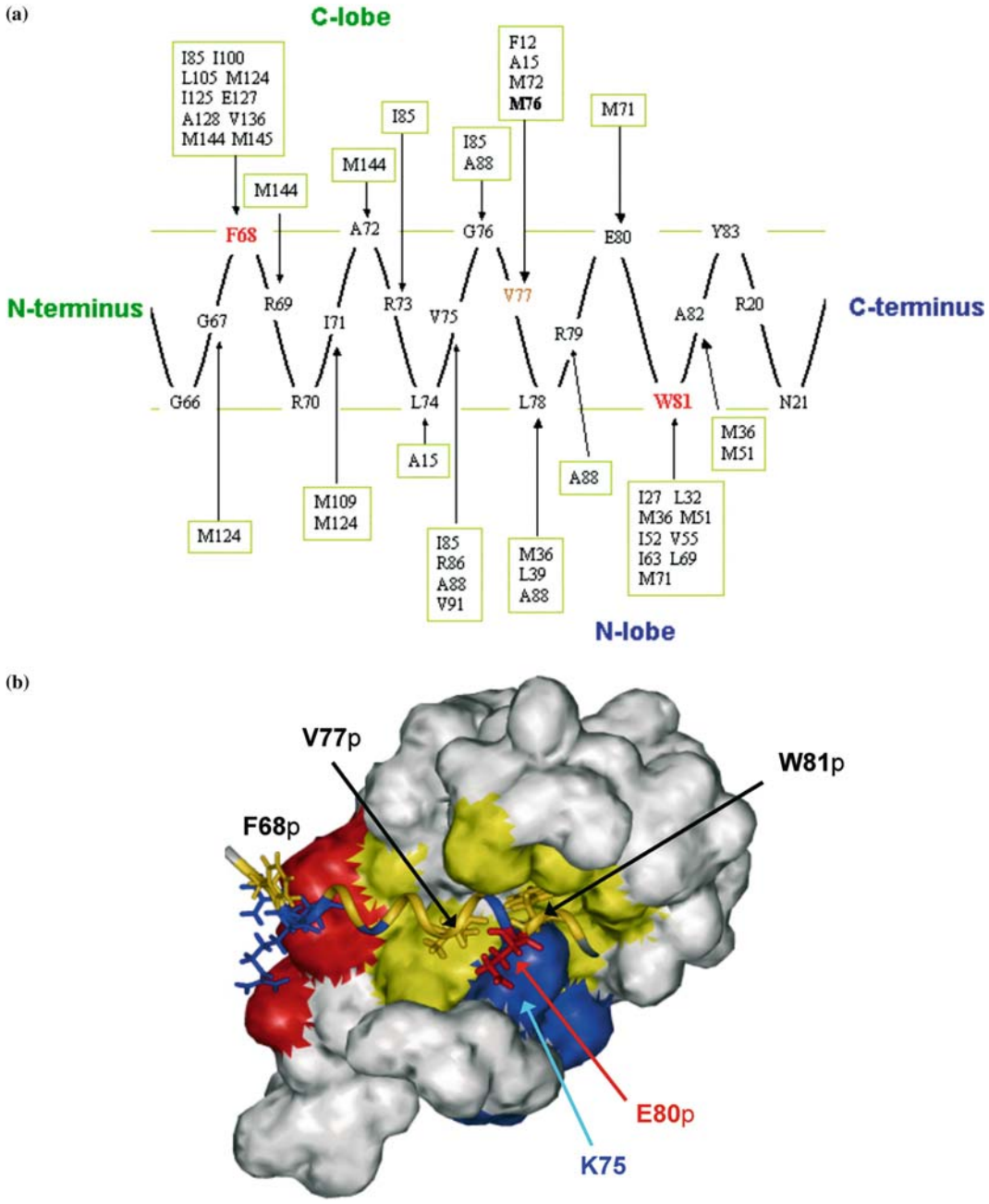

Figure 3. The interaction between CaM and bOCNCp. (a) Schematic representation of observed peptide-CaM NOEs. (b) Surface representation of the N-lobe of CaM showing hydrophobic and electrostatic complementarity between CaM and bOCNCp. Hydrophobic residues are shown in yellow, positive charges in blue and negative in red.

already described unfavourable interaction between E498 in eNOSp and E14 in CaM. Moreover, the presence of a bulky residue in position 10 (relative to F) for both bOCNCp and eNOSp elongates Helix IV and leaves a very short linker. This feature is absent in the smMLCKp complex, probably since it presents a less bulky alanine residue in the corresponding position (Figure 1). Finally, in the bOCNCp complex, Helix I is clearly shifted towards the outside if compared with the

Table 2. Interhelical angles and RMSD to CaM–bOCNCp complex

	CaM–smMLCK	CaM–eNOS	CaM–bOCNCp
PDB entry	1CDL	1NIW	1SY9
I–II	90° ± 3°[a]	79° ± 2°[a]	93° ± 3°[b]
III–IV	96° ± 3°	74° ± 4°	94° ± 2°
V–VI	84° ± 2°	82° ± 1°	79° ± 2°
VII–VIII	81° ± 2°	92° ± 5°	96° ± 2°
RMSD (res. 7–74)	1.7	1.8	
RMSD (res. 82–146)	1.3	1.0	
RMSD (res. 7–74, 82–146)	2.0	2.2	
RMSD (overall)	1.9[c]	2.2[d]	

SD refers to: [a]the four molecules of the asymmetric unit. [b]the 20 lowest-energy NMR structures. [c]Residues 7–74, 82–146, 800–813. [d]residues 7–74, 82–146, 496–507.

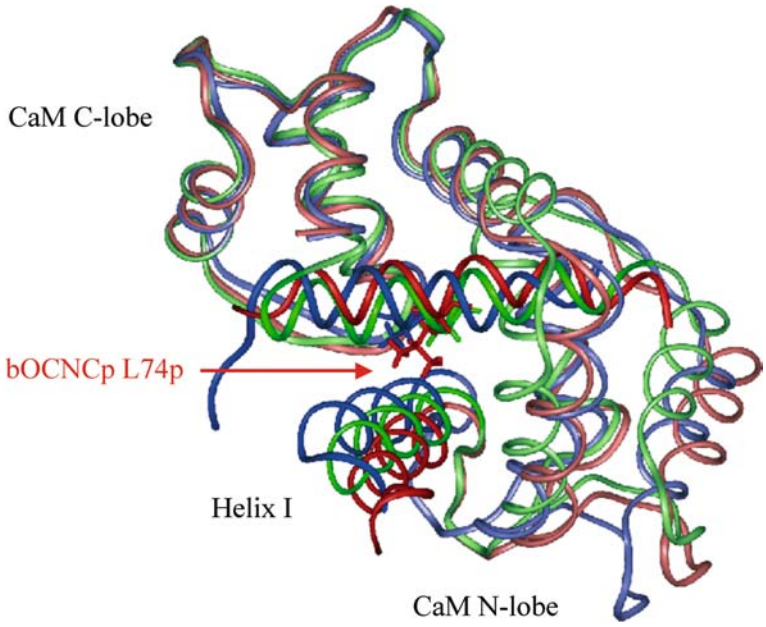

Figure 4. Superposition of the three 1–14 complexes, bOCNC (red), smMLCK (blue) and eNOS (green): the three structures are aligned by super-imposing the C-terminal part of CaM (residues 83–145). The bulky Leucine 74p of bOCNCp, responsible for the shift of Helix I, and the corresponding Alanine in smMLCKp and eNOSp are shown.

position observed in eNOSp and smMLCKp complexes, due to the presence of L74p. The other two peptides have a less bulky alanine in this position (see Figure 1), which can be accommodated to leave Helix I more tightly packed against the peptide. Large differences in the relative orientation of Helix I, of the order of 26°, were already observed between the solution and crystal structures of free CaM (Chou et al., 2001), suggesting that this helix can be oriented in different ways to optimize CaM binding to different targets.

Backbone dynamics of the CaM–bOCNCp complex

^{15}N relaxation times (T1 and T2) and the steady-state ^{1}H–^{15}N NOE were measured at 70.94 MHz ^{15}N base frequency (Figure 5a). Figure 5a shows also the fitted S^2 parameters for bound CaM. Residues belonging to the eight helices show regular values for the global order parameter S^2, of the order of 0.85–0.90. Figure 5b shows regions of CaM affected by fast (red), slow (blue) and combined motions (green). The latter is hypothesized

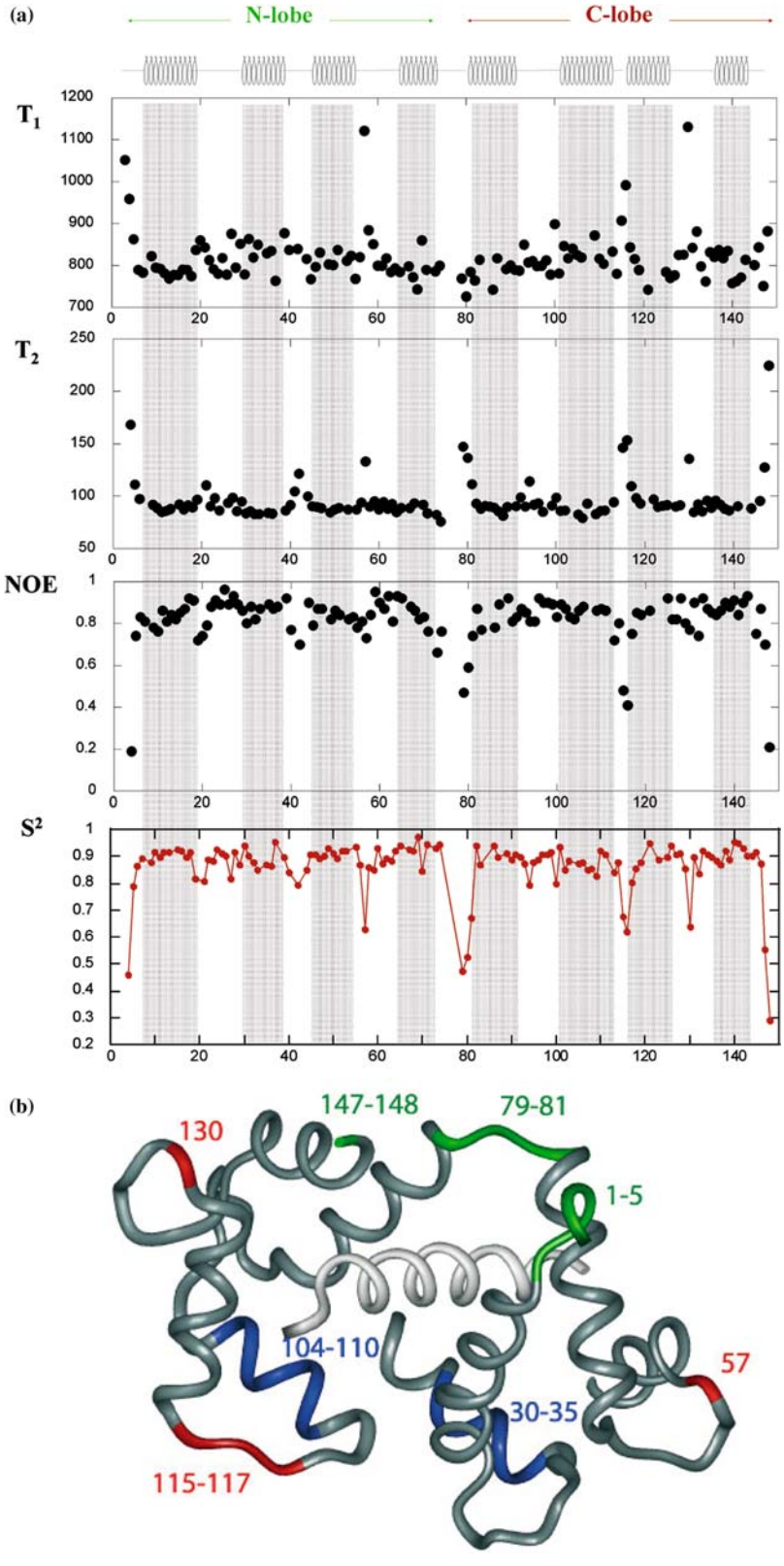
(a)
N-lobe
C-lobe
T1
T2
NOE
S2
(b)
130
147-148
79-81
1-5
104-110
57
30-35
115-117

for residues 79–81, in the central linker connecting the two lobes, and for the N-terminal and C-terminal residues. These residues show long T_2, but a value of T_1 that is close to that of the structured regions. A fitting with a model considering only fast motions (model (c) see Materials and methods) gave only poor results. Therefore, we attempted the use of the 'extended' model-free method (Clore et al., 1990b). In this case, both a slow and a fast internal motions are assumed, leading to a three-parameters model, if τ_f is set to 0 and τ_m is fixed. Clearly, the results obtained using this model with only three observables have to be analyzed with caution and a more quantitative description of the internal motions would require a larger experimental data set. However, if one just aims at the detection of the occurrence of molecular flexibility in these regions, the present analysis is sufficient.

Our study of the flexibility of CaM bound to a target peptide demonstrates the presence of dynamical fluctuations in the Ca^{2+}-binding loops, in the relatively long loops connecting the EF-hand motifs, and in the short linker. In this latter case, the overlap of the peaks doesn't allow the measurement of relaxation rates for some of the residues in the 74–77 region. The already mentioned NOEs detected for M76 and the presence of the typical NOEs for a helical conformation for residues 75–77 are an indication of some sort of structural rigidity. On the other hand, the conformation of the linker resembles that found in the eNOSp complex (Aoyagi et al., 2003), where relative high temperature factors were obtained for residues in the 74–82 region (see below). Although we have a second electrostatic interaction involving K75 and E80p, one cannot rule out the occurrence of some residual flexibility in the K75–K77 region.

The observed flexibility for the Ca^{2+} binding loops and the linkers between the two EF-hand motifs can be related to the dynamical behaviour detected for free CaM (Chou et al., 2001). The analysis of a very large set of RDC provided evidence for the scissor-like motions within each EF-hand. We think that the observed flexibility in the Ca^{2+} binding loops and loops connecting the EF-hand motifs in the CaM–bOCNCp complex are residual movements that remain after more fixed orientations of the helices are imposed by the interaction with the target.

Use of RDCs to determine CaM–b–OCNC binding mode

CaM–bOCNCp represents an example of a 1:1 CaM complex with a peptide not belonging to the kinase family for which RDC values are available. Hence it can be a stringent test for the ability of RDC to detect calmodulin binding, using as templates the three complexes of kinases fragments plus the eNOSp complex. In the case of the CaM–smMLCKp and CaM–eNOSp complexes four different molecules are found in the asymmetric unit. The molecules with the highest temperature factors were discarded, whereas the one showing the best agreement with our experimental data was retained.

A best-fit molecular alignment tensor was obtained by using the PALES program (Zweckstetter and Bax, 2000). In a first run the RDC method was performed following the original description of Mal et al. (2002). In this case only residues belonging to putatively unstructured regions, like 1–5, 73–84 and 145–148, were excluded from the calculation. To test the agreement between calculated and experimental RDC values we used the quality factor Q (Cornilescu et al., 1998), that approaches to 0 when a perfect matching is obtained, and is more sensitive than the regression coefficient R^2 to detect deviations between experimental and theoretical data (Ottiger and Bax, 1999). The Q values obtained using the above mentioned crystal structures as references are relatively high and similar to each other (0.33, 0.35, 0.32 and 0.33) (Figure 6a). Analysis of the correlations derived for individual domains (N and C) are also shown. The comparison of the correlations for the whole protein and for the two lobes separately shows that, when using the smMLCK or the eNOS complexes as templates, there is no

◀

Figure 5. (a) Plots as a function of residue number of ^{15}N T_1, T_2 and NOE measured at 700 MHz, and the calculated global order parameter S^2. The eight helices of CaM are highlighted. (b) Color-coded backbone representation indicating the dynamic hotspots of CaM: regions affected by fast (red), slow (blue) and combined motions (green) are shown.

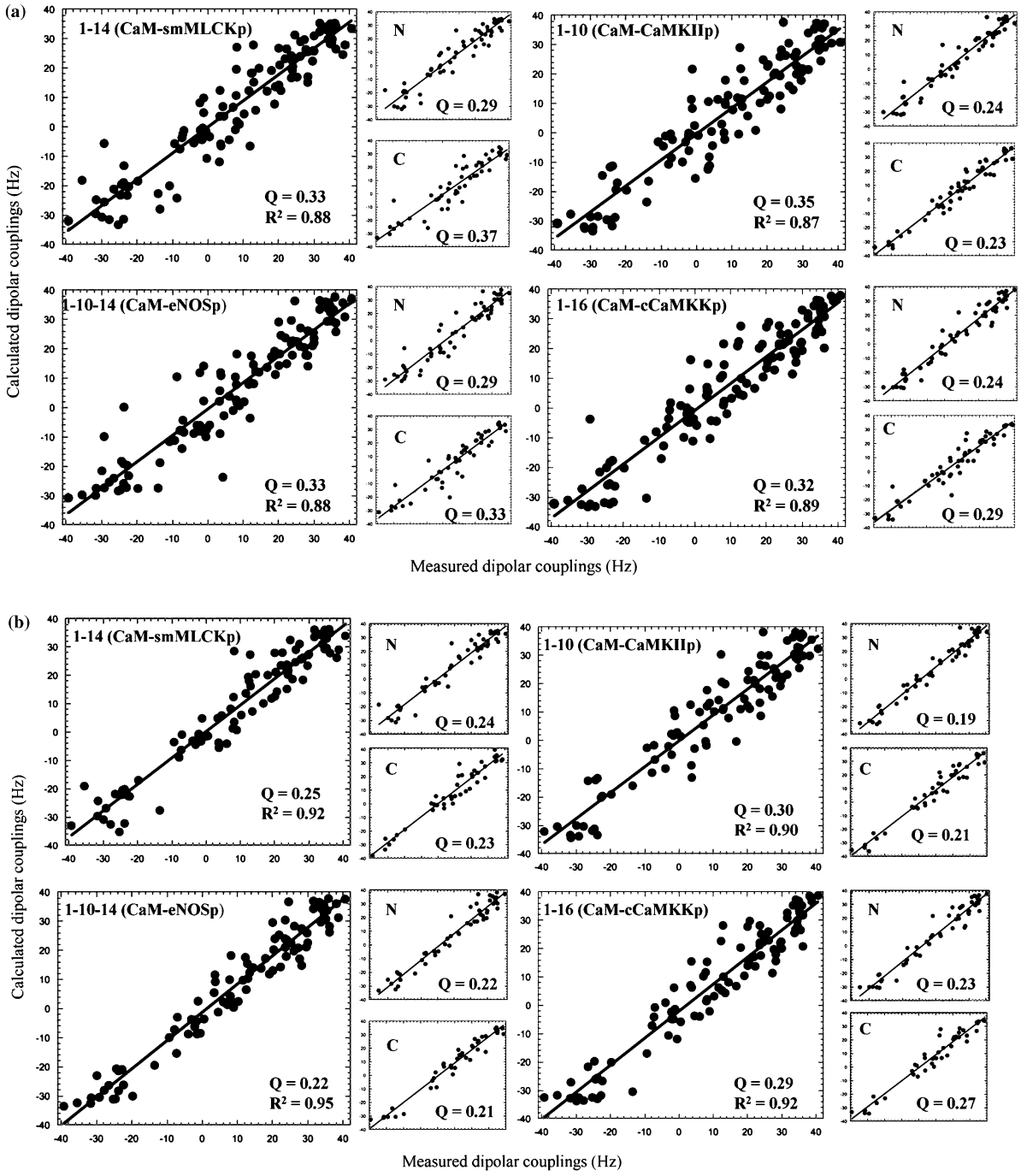

Figure 6. Correlations between experimentally measured ^{1}H–^{15}N RDCs of the CaM–bOCNCp complex and the best-fit RDC values calculated with the CaM–CaMKIIp (1–10), CaM–smMLCKp (1–14), CaM–cCaMKKp (1–16) and CaM–eNOS (1–10–14) crystal structures. The correlation coefficient R^2 and quality factor Q for each complex are given in the plots. The correlations derived for individual domains (N and C) of CaM are shown in the small panels to the right. (a) using the RDC dataset comprising residues 6–72 for the N-terminal domain, and 85–144 from the C-terminal domain. (b) excluding regions showing flexibility (residues 1–5, 40–44, 57–61, 113–117, 130–133, 145–148).

significant difference between the observed Q for the separated lobes and for the total structure, while for the 1–10 and 1–16 structures a lower Q is obtained for the separate lobes than for the overall structure. In fact, the coefficient χ^2/σ^2, which is the square of the ratio between the rmsd of the global fit χ and the average rmsd of the separated lobe fit σ (Mal et al., 2002), is close to 1.1 for the two 1–14 complexes and close to 2.2 and 1.6 for the 1–10 and 1–16 complexes, respectively. The *F*-test already described was used to demonstrate the statistical significance of the observed differences in Q values. It indicates that the difference between the fitting of the 1–14 and the other two complexes presents associated probabilities of occurring by chance of 0.003 and 0.03, respectively. Both numbers are below the significance level used in the test (0.05), indicating that the differences are statistically significant.

Although the structure of CaM–bOCNCp clearly indicates that it belongs to the 1–14 family, we observe high Q values also when using complexes of CaM with smMLCKp and eNOSp. One possible source for the high Q value observed in the four cases is the presence of flexibility in the CaM–bOCNCp in solution, or disorder in the crystal state for the template structures.

High temperature factors for the C_α atoms of the four complexes were observed for the two loops connecting the two EF-hand motifs, namely residues 40–45 and 113–117 (see supplementary material). Higher temperature factors were reported for the N-lobe than the C-lobe, and in particular for residues belonging to the Ca^{2+}-binding loops (21–30 and 58–65). The 1–16 complex also shows relatively high factors for the C-lobe Ca^{2+}-binding loops (94–99 and 129–137). Comparison of these temperature factors with the S^2 plot of Figure 5a reveals a clear correlation between the disorder or thermal motion observed in the crystalline state and the degree of flexibility observed in solution for the CaM–bOCNCp complex.

As far as the solution structure is concerned, only motions with large associated amplitudes (>15°) are expected to have a significant influence on the measured RDCs (Tolman et al., 2001). Following the S^2 graphic (Figure 5a, b) such motions are expected to occur only for the first and last residues of the protein, the residual linker (residues 79–81) and the loop 113–117 in the C-lobe, plus residues A57 and I130 in the second and fourth Ca^{2+}-binding loops, symmetrically located in the two lobes. The back calculated RDCs upon exclusion of these residues using the four complexes as templates are shown in Figure 6b.

The agreement for the calculation of the separate lobes is highly improved with respect to the use of the whole dataset, and is quite homogeneous with respect to the four complexes. Q values of about 0.22 and 0.23 for the N- and C-lobes, respectively were obtained.

The global fit improved significantly only for the two 1–14 complexes, whereas the 1–10 and the 1–16 complexes still show a high value of Q. This result is in agreement with the fact that the binding mode of bOCNCp belongs to the 1–14 family, as the χ^2/σ^2 parameter clearly indicated using the whole set of RDC. Although the fitting is clearly improved by not considering flexible regions, the obtained Q values are still higher to that observed for the kinase fragments analysis (Mal et al., 2002). A closer look at those RDCs deviating from the experimental values reveals some clues about the differences among the 1–14 complexes. Residues like T44 and Q42, belonging to the loop connecting the two EF-hands in the N-lobe deviate from the expected values in the smMLCKp and eNOSp complexes, respectively. The same observation holds for G25 and I27, both belonging to the first Ca^{2+}-binding loop. The two regions, however, show high temperature factors in the two crystals, and cannot be taken as reliable probes of conformational differences. Deviations in the RDC values were also observed for G98 in the smMLCKp complex, which is allocated in the third Ca^{2+}-binding loop. For this region, neither high temperature factors were reported, nor large amplitude motions were detected in solution. The difference can then be attributed to a conformational divergence between the structures. More easily interpretable is the discrepancy observed with the calculated RDC values for E6 and I9 of the eNOSp complex. In fact, the already cited shift of the first helix, caused by the presence of a negative charge in the peptide, can be safely used as the main reason for the deviations in the orientations of Helix I NHs in the crystal with respect to the bOCNCp complex.

Conclusions

The bOCNCp complex revealed a second example, along with the recently described eNOSp complex, in which the linker plays an active role in the target interaction. The CaM–bOCNCp structure shows for the first time the participation of CaM positively charged residues in electrostatic interactions with a negatively charged residue of the target. In fact, there are only two other known structures of CaM complexed with targets presenting negatively charged residues: eNOSp (Aoyagi et al., 2003) and GADp (Yap et al., 2003). In the first case, no electrostatic interaction with CaM was found for E498, whereas in the second case that shows two bound peptides, negatively charged residues of GADp interact with positively charged residues of the same peptide or with the second bound peptide. The interaction between E80p and K75 in the bOCNCp complex seems to favour the antiparallel orientation of the peptide, but it is not clear if it adds to the observed high affinity. Recent studies suggest that electrostatic interactions between CaM and peptides are more likely to be used to discriminate against unbound proteins rather than to increase the affinity for any particular target protein (André et al., 2004).

Finally, the present study confirms that RDC analysis can provide an excellent and quick way to assess the binding mode of CaM to targets not belonging to the kinase family. The major difference with the results of the latter, is that, also for high Q values, the χ^2/σ^2 parameter is still a sensitive estimator of the relative orientation of the two lobes. Moreover, the ^{15}N relaxation study allowed to establish regions of flexibility that are present in the complex with bOCNCp. These regions correlate well with those having relative high temperature factors in the crystal structure of other CaM complexes, indicating that in addition to the linker region, also the Ca^{2+}-binding loops and the loops connecting the EF-hands motif remain flexible. This flexibility can be regarded as a residual mobility compared to that observed in free CaM and it represents the basic condition of the remarkable conformational plasticity used by this protein to adapt itself to a very broad series of targets with different sequences.

The coordinates of the CaM–bOCNCp structure have been deposited in the Protein Data Bank under the code 1SY9.

Supplementary material available

Figure giving the comparison of the global order parameter S^2 for CaM in the bOCNC complex with the temperature factors for the C_α atoms of the MLCK and eNOS complexes. This material is available at http://dx.doi.org/10.1007/s10858-005-0165-1.

Acknowledgements

We thank Dr Renzo Bazzo for helpful discussions about the manuscript and Dr Gaetano Barbato (IRBM, Rome) for T_2 data of free calmodulin. The technical assistance of Mr. Fabio Bertocchi is gratefully acknowledged.

References

André, I. Kesvatera, T. Jonsson, B. Akerfeldt, K.S. and Linse, S. (2004) *Biophys. J.*, **87**, 1929–1938.
Aoyagi, M. Arvai, A.S. Tainer, J.A. and Getzoff, E.D. (2003) *EMBO J.*, **22**, 766–75.
Babu, Y.S. Bugg, C.E. and Cook, W.J. (1988) *J. Mol. Biol.*, **204**, 191–204.
Barbato, G. Ikura, M. Kay, L.E. Pastor, R.W. and Bax, A. (1992) *Biochemistry*, **31**, 5269–5278.
Bax, A. (2003) *Protein Sci.*, **12**, 1–16.
Bax, A. Kontaxis, G. and Tjandra, N. (2001) *Methods Enzymol.*, **339**, 127–174.
Bewley, C.A. Gustafson, K.R. Boyd, M.R. Covell, D.G. Bax, A. Clore, G.M. and Gronenborn, A.M. (1998) *Nat. Struct. Biol.*, **5**, 571–578.
Brunger, A.T. (1992) Yale University Press, New Haven.
Bryce, D.L. and Bax, A. (2004) *J. Biomol. NMR.*, **28**, 273–87.
Chou, J.J. Li, S. Klee, C.B. and Bax, A. (2001) *Nat. Struct. Biol.*, **8**, 990–997.
Clore, G.M. Driscoll, P.C. Wingfield, P.T. and Gronenborn, A.M. (1990a) *Biochemistry*, **29**, 7387–7401.
Clore, G.M., Szabo, A., Bax, A., Kay, L.E., Driscoll, P.C. and Gronenborn, A.M. (1990b) *J. Am. Chem. Soc.* 4989–4991.
Clore, G.M. and Gronenborn, A.M. (1998) *Proc. Natl. Acad. Sci. USA*, **95**, 5891–5898.
Clore, G.M. Gronenborn, A.M. and Tjandra, N. (1998) *J. Magn. Reson.*, **131**, 159–162.
Clore, G.M. and Garrett, D.S. (1999) *J. Am. Chem. Soc.*, **121**, 9008–9012.
Cornilescu, G. Marquardt, J.L. Ottiger, M. and Bax, A. (1998) *J. Am. Chem. Soc.*, **120**, 6836–6837.
Delaglio, F. Grzesiek, S. Vuister, G.W. Zhu, G. Pfeifer, J. and Bax, A. (1995) *J. Biomol. NMR*, **6**, 277–293.
Farrow, N. Muhandiram, D.R. Singer, A.U. Pascal, S.M. Kay, C.M. Gish, G. Shoelson, S.E. Pawson, T. Forman-Kay, J.D. and Kay, L.E. (1994) *Biochemistry*, **33**, 5984–600.
Fischer, M.W. Losonczi, J.A. Weaver, J.L. and Prestegard, J.H. (1999) *Biochemistry*, **38**, 9013–9022.

Hansen, M.R. Mueller, L. and Pardi, A. (1998) *Nat. Struct. Biol.*, **5**, 1065–1074.
Ikura, M. Clore, G.M. Gronenborn, A.M. Zhu, G. Klee, C.B. and Bax, A. (1992) *Science*, **256**, 632–638.
Ikura, M. and Bax, A. (1992) *J. Am. Chem. Soc.*, **114**, 2433–2440.
Johnson, B. and Blevins, R.A. (1994) *J. Biomol. NMR*, **4**, 603–614.
Kay, L.E. Torchia, D.A. and Bax, A. (1989) *Biochemistry*, **28**, 8972–8979.
Kurokawa, H. Osawa, M. Kurihara, H. Katayama, N. Tokumitsu, H. Swindells, M.B. Kainosho, M. and Ikura, M. (2001) *J. Mol. Biol.*, **312**, 59–68.
Laskowski, R.A. Rullmannn, J.A. MacArthur, M.W. Kaptein, R. and Thornton, J.M. (1996) *J. Biomol. NMR*, **8**, 477–86.
Lee, W. Revington, M.J. Arrowsmith, C. and Kay, L.E. (1994) *FEBS Lett.*, **350**, 87–90.
Lipari, G. and Szabo, A. (1982) *J. Am. Chem. Soc.*, **104**, 4546–4559.
Liu, M. Chen, T.-Y. Ahamed, B. Li, J. and Yau, K.-W. (1994) *Science*, **266**, 1348–1354.
Losonczi, J.A. Andrec, M. Fischer, M.W. and Prestegard, J.H. (1999) *J. Magn. Reson.*, **138**, 334–342.
Mal, T.K. Skrynnikov, N.R. Yap, K.L. Kay, L.E. and Ikura, M. (2002) *Biochemistry*, **41**, 12899–12906.
Meador, W.E. Means, A.R. and Quiocho, F.A. (1992) *Science*, **257**, 1251–1255.
Meador, W.E. Means, A.R. and Quiocho, F.A. (1993) *Science*, **262**, 1718–1721.
Molday, R.S. (1996) *Curr. Opin. Neurobiol.*, **6**, 445–452.
Orekhov, V.Y. Nolde, D.E. Golovanov, A.P. Korzhnev, P.M. and Arseniev, A.S. (1995) *Appl. Magn. Reson.*, **9**, 581–588.
Orsale, M. Melino, S. Contessa, G.M. Torre, V. Andreotti, G. Motta, A. Paci, M. Desideri, A. and Cicero, D.O. (2003) *FEBS Lett.*, **548**, 11–16.
Osawa, M. Tokumitsu, H. Swindells, M.B. Kurihara, H. Orita, M. Shibanuma, T. Furuya, T. and Ikura, M. (1999) *Nat. Struct. Biol.*, **6**, 819–824.
Ottiger, M. and Bax, A. (1999) *J. Mol. Biol.*, **13**, 187–191.
Ottiger, M. Delaglio, F. and Bax, A. (1997) *J. Magn. Reson.*, **131**, 373–378.
Putkey, J.A. Slaughter, G.R. and Means, A.R. (1985) *J. Biol. Chem.*, **260**, 4704–4712.
Rhoads, A.R. and Friedberg, F. (1997) *FASEB J.*, **11**, 331–340.
Tjandra, N. Kuboniwa, H. Ren, H. and Bax, A. (1995) *Eur. J. Biochem.*, **230**, 1014–1024.
Tjandra, N. Omichinski, J.G. Gronenborn, A.M. Clore, G.M. and Bax, A. (1997) *Nat. Struct. Biol.*, **4**, 728–732.
Tolman, J.R. Al-Hashimi, H.M. Kay, L.E. and Prestegard, J.H. (2001) *J. Am. Chem. Soc.*, **123**, 1416–1424.
Varnum, M.D. and Zagotta, W.N. (1997) *Science*, **278**, 110–113.
Vetter, S.W. and Leclerc, E. (2003) *Eur. J. Biochem.*, **270**, 404–414.
Yap, K.L. Kim, J. Truong, K. Sherman, M. Yuan, T. and Ikura, M. (2000) *J. Struct. Funct. Genomics.*, **1**, 8–14.
Yap, K.L. Yuan, T. Mal, T.K. Vogel, H.J. and Ikura, M. (2003) *J. Mol. Biol.*, **328**, 193–204.
Zweckstetter, M. and Bax, A. (2000) *J. Am. Chem. Soc.*, **122**, 3791–3792.